Bio-Based Type I Photoinitiator: Carbon Dots with Oxygen Tolerance

Wang, Qunying, Niederrhein University of Applied Sciences, Germany
Chen, Zhijun, Northeast Forestry University, China
Luo, Xiongfei, Northeast Forestry University, China
Pang, Yulian, Hubei Gurun Technology Co., LTD, China
Strehmel, Bernd, Niederrhein University of Applied Sciences, Germany
Corresponding author: bernd.strehmel@hs-niederrhein.de

***Key words**:* Radical Photopolymerization; Carbon Dots; Type I Photoinitiator; Polymer networks; Oxime Ester
***Discipline**:* Advances in Sciences of Paints, Adhesives, Inks

Introduction

Photopolymerization[1] has received great interest in diverse fields such as 2D[2] and 3D patterning[3], information recording based on holography[4], medicine[5], chemical drying of coatings[6,7], and processing of electronic materials[8] - just to name a few fields of the diverse applications. Particularly, UV-initiated traditional free radical photopolymerization has moved into the focus because it enables fast solidification of organic coatings. It can be seen as a door opener to introduce new energy-saving technologies in inline manufacturing. Photopolymerization has continuously grown worldwide with nearly no interruption even in pandemics between 2020-2022[9]. Thus, Europe, the USA, and Asia showed a growth in production volume, depending on geographic location, between 5-8%. This rate will continuously grow due to the demand of the society to replace older chemical technologies with modern photonic techniques related to chemical drying[6,7].

Light-sensitive materials, such as photoinitiators (**PI**), require additional care in case the processed materials are directly in contact with humans. Users demand to develop more migration-resistant materials to minimize the risk on top of the surface where it could directly harm humans[10]. Binding the light-sensitive group at a polymer chain presents one possibility[11] to reduce diffusion that causes migration[12].

Photoinitiating systems generating initiating radicals according to a unimolecular homolytic bond cleavage mechanism have received great attention in recent decades[1a,b,e-h]. Here, materials following a homolytic bond cleavage possess the widest distribution. Particularly, the distribution of phosphine oxide-based **PI**s has continuously grown. Their worldwide production occupies an increasing volume of 4 to 7 t between 2020-2022[9]. Nevertheless, this also showed that under some circumstances, the materials caused issues related to health because the **PI** migrated in the light-processed material. This demanded the development of alternatives, which should be economically affordable, less harmful, and more migration resistant. Oxime esters, competitively developed in the last decades, were seen as alternatives[1b,13].

Efforts exist to introduce sustainable **PI**s based on traditional free radical polymerization into the field[3d, 14]. Nevertheless, their origin should not relate to the food chain. Two-component systems, disclosed as Type II initiators[1a-b], were successfully introduced. Their use requires a second component[1a-b,15], which is typically not migration resistant. These systems were found to be used in photocatalytic cycles in controlled radical polymerization protocols[16], and to clean wastewater[15c]. The latter demonstrates the potential for multiple uses of such materials, namely as initiators for free radical polymerization, and as catalysts for environmental protection. On the other hand, photosensitive materials typically do not bleach in catalytic cycles. This shortens their wider use in photopolymerization technologies where bleaching enables photoinduced crosslinking even of samples exhibiting larger thickness; that

starts ≳100 μm and successfully works up to some centimeters[17]. Here, Type I **PI**s dominate because the unimolecular bond cleavage irreversibly results in bleaching. This almost works well if the absorption of the photoproducts shows hypsochromic shifted absorption with respect to the substrate.
Sustainable and more migration-resistant **PI**s will enable the start of a new chapter in the field of light-mediated photopolymerization. Attention shall be paid to carbon dots as a new type of novel carbon nanomaterials with an average size of less than 10 nm. Both, hydrothermal and solvothermal procedures easily enable synthesis from sustainable precursors[18]. Until now, carbon dots have exhibited great potential for use in bioimaging[19], as photocatalysts in synthetic procedures[20], 3D printing[3], and photothermal conversion[21]. The practical demand addresses these materials to enable technologies to operate in short time frames that must also cover the millisecond time frame[2a].

Results and Discussion
Motivated by this, we introduce a Type I UV photoinitiator comprising a sustainable carbon dot as part of the conjugated system for the first time. To this end, carbon dots were first synthesized from sustainable furfural following a solvothermal procedure (Figure 1). The surface of the carbon dots comprised aldehyde groups, which reacted with hydroxylamine. The as-obtained oxime of the carbon dots reacted further with an acid chloride, resulting in photocleavable carbon dot oxime ester (**CD-PI**). This structure similarly reminds that of a dandle-ion-like pattern introduced with NIR-sensitive materials[1i].
Following the example in Figure 1, this can generate an iminyl radical and an acyloxy radical. The latter fast decomposes to CO_2 and the respective aryl radical. Both reactive radicals can initiate traditional free radical polymerization of multi-functional acrylic esters resulting in the formation of crosslinked polymer. Experiments pursued compare reactivity in radical polymerization with traditional Ethyl (2,4,6-trimethyl benzoyl) phenyl phosphinate **PI** (**TPO-L**), which represents state-of-the-art in the field of UV-initiated free radical polymerization in practice.
Nevertheless, **TPO-L** can migrate out of a chemically dried coating due to the lower molecular weight, while the high mass of **CD-PI** suppresses this undesirable phenomenon. Furthermore, as shown in Figure 1, this type of **PI** can generate several iminyl radical radicals on the surface of the **CD**, which can additionally initiate radical polymerization. Thus, the **CD-PI** could be additionally seen as a source to form composite-like materials, particularly at higher concentrations. This will impact the material properties such as network formation.
FTIR spectra monitored the steps of the synthesis procedure of **CD-PI** (Figure S2). After decorating carbon dots with hydroxylamine, signals of aldehyde at 1674 cm^{-1} disappeared and new signals at 1643 cm^{-1}, referred to as the -C=N-, were observed, indicating the successful reaction. Additionally, signals of -OH exhibited a significant decrease after esterification, suggesting the benzoyl chloride successfully reacted with surficial hydroxyl moieties. Chemical titration provided information regarding the reaction of hydroxyl moieties in the oxime compared to before and after esterification[22]. The amount of hydroxyl groups in **CD** oxime decreased from 3.25 $mmol \times g^{-1}$ to 1.25 $mmol \cdot g^{-1}$ after the reaction. Resulting in ~2 $mmol \cdot g^{-1}$ oxime ester moieties in **CD-PI**. The conversion yield of the entire process was ~5% in a three-step synthesis. Future work will focus on improving the process.

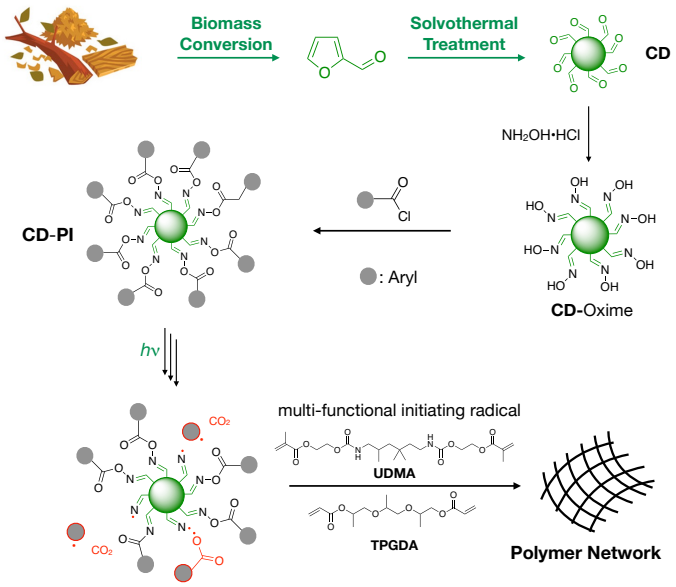

Figure 1. Schematic illustration of the preparation of **CD-PI** from furfural available from hemicellulose, where wood serves as a source. Solvothermal reaction conditions result first in the formation of carbon dots comprising aldehyde groups on their surface. Additional treatment with hydroxylamine yields the respective oxime, which reacts with acid chloride to the target material, the oxime ester. Dispersion of **CD-PI** in the respective monomer mixture results in the polymer network by exposure to UV light.

TEM images (Figure 2a, left and right) show a size of ≈3 nm for **CD-PI**, which appears similar to the carbon dots and carbon dots-based oxime (Figure S3). In addition, **CD-PI** exhibited a typical signal of 21.3 degrees in the XRD pattern, which was similar to the carbon dots and carbon dots-based oxime (Figure 2b). These results demonstrated that surficial decoration did not alter the carbon core structures of **CD-PI** inheriting from the carbon dots. XPS analysis showed that **CD-PI** possessed C, N and O elements (Figure S4) and exhibited surficial moieties of C=C, C=N, C=O and O=C-O. These results were consistent with FTIR analysis of **CD-PI** (Figure S2).

Consecutive experiments of **CD-PI** dispersed in different solvents focused to select an appropriate solvent to prepare proper dispersion systems. Measurement of the extinction coefficient of **CD-PI** showed acetonitrile resulted in the best performance while the selection of water indicated the worst performance (Table S1). Thus, the photoreaction of **CD-PI** was determined using acetonitrile. To verify the light-sensitive response upon UV exposure, UV-Vis. spectra of **CD-PI**, whose absorbance decreased, were recorded after different exposure times (Figure 2c).

Interestingly, UV-Vis spectra of **CD-PI** measured with deoxygenation exhibited fewer changes compared to samples exposed to an air-saturated solution (Figure S5). A complex mechanism involving oxygen in the formation of reactive species could explain this phenomenon. More important, CO_2 release from the solution of **CD-PI** was observed during the UV irradiation (Figure 2d). This resulted in decolorization of a slight alkaline phenolphthalein solution approving the validity of the mechanism shown in Figure 1. A comparison of FTIR spectra of **CD-PI** recorded at different exposure times indicated a change of signals related to the =NO)–(C=O moiety (Figure S6). ESR spectra of trapped photolytic-generated radicals showed the formation of active radicals released by the **CD-PI** (Figure 2e). The spectra indicated a splitting of A_N = 14.4 G and A_H = 2.1 G of the radical formed by the scavenger *N*-*t*-butyl-□-phenylnitrone (PBN). This agrees with data of the phenyl radical trapped with PBN (A_N = 14.4 G, A_H = 2.1 G)[23]. Simulated ESR spectra evidenced similarity with experimental data (Figure S7).

Notably, TEM images of **CD-PI** were analyzed before and after UV irradiation (Figure S8). No obvious size change was observed, indicating the carbon cores were reserved in **CD-PI**. Additionally, the XRD pattern of **CD-PI** also did not obviously change before and after UV irradiation suggesting the unaltered structure of carbon cores (Figure S9).

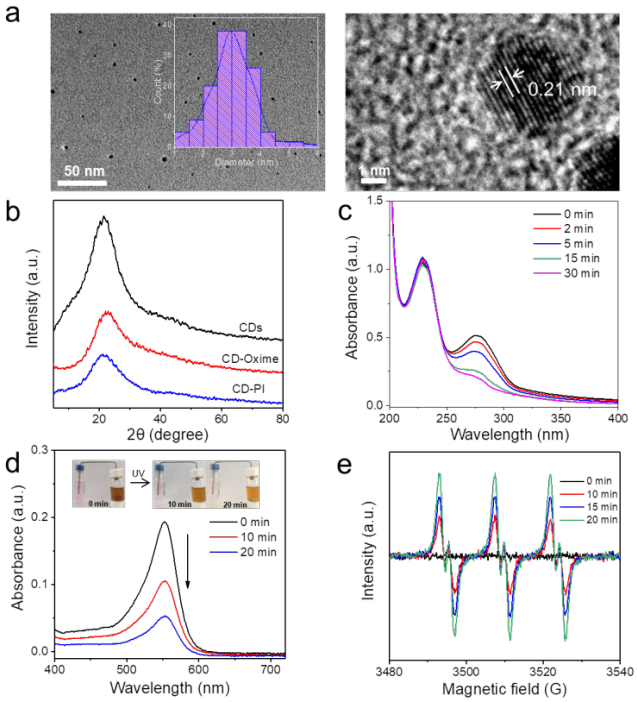

Figure 2. a) TEM image of CD-PI (Inset: Size distribution of CDs (left)) high-resolution TEM image of CD-PI (right); b) XRD pattern of **CD**s (black line), **CD**-Oxime (red line) and **CD-PI** (blue line); c) UV-Vis spectra of **CD-PI** in acetonitrile upon UV irradiation for a different time (0 - 30 min); d) UV-Vis spectra of phenolphthalein solution obtained upon of a solution of **CD-PI** ($c_{\mathbf{CD\text{-}PI}}$ = 555.6 mg/L, c_{Na2CO3} = 16.8 mg/L) in acetonitrile (Inset: Digital images of color change of the solution upon UV irradiation); e) ESR spectra of trapped radicals upon exposure of **CD-PI** upon UV irradiation for a different time, $c_{\mathbf{CD\text{-}PI}}$ = 10 mg/mL, c_{PBN} = 5.64×10^{-3} M. All the UV sources were 365 nm emitting (c-d with an intensity of 50 mW/cm^2 and e with an intensity of 20 mW/cm^2).

Encouraged by the results, photoinitiating experiments were pursued using **CD-PI** dispersed in a mixture of **UDMA** and **TPGDA** (60:40, wt). This ratio was found as the most effective as concluded by the mechanical performance of the cured samples obtained in stress-strain experiments (Figure S10). In addition, a series of alternative monomer mixtures comprising were additionally included comprising either Hexamethylene diacrylate, Poly(ethylene glycol) diacrylate, 2-Hydroxyethyl acrylate (EHA) or 1,1,1-Trimethylol propane triacrylate (TMPTA). They were also successfully photocured with the assistance of **CD-PI** (Figure S11). Since each of these mixtures will result in distinct crosslinked structures caused by the different functionalities of the monomers, the mixture of **UDMA** and **TPGDA** was chosen for comparison with previous investigations to evaluate **CD-PI**.
Real-time FTIR spectroscopy monitored double bond conversion (Figure 3a). Obviously, **CD-PI** tolerated a better change in **PI** concentration compared to the reference **TPO-L**. A concentration of 1 wt% resulted in a final conversion of 71% for both **CD-PI** and **TPO-L**. Further concentration increases to 2 wt% approached a final conversion to 76 % and 86% for **CD-PI** and **TPO-L**, respectively. More interesting appears the fact that **CD-PI** significantly tolerates better the reduction of **PI**-reduction compared to the low molecular weight **PI TPO-L**. The final conversion obtained was similar while lower concentration resulted, as expected, in a later starting of the process. Here, conversion significantly increased after 20 s compared to data with 1 wt% loading (4 s). Surprisingly, **CD-PI** also showed acceptable photoinitiating

speed in the presence of oxygen (Figure **S12**) although the overall rate was higher under anaerobic conditions. Traditional photoinitiators do not show any oxygen tolerance. Reactive oxygen species generated by carbon dots in the **CD-PI** can cause such phenomena[24]. It may indicate the involvement of triplet states contributing to the formation of singlet oxygen. Oxidation of specific substrates by this species results in consumption of inhibiting oxygen as previously discussed in photo-RAFT protocols[25]. Nevertheless, these results demonstrate a distinct behavior of the two distinct **PI**s, namely **CD-PI** and **TPO-L**, during the crosslinking process. Of course, **TPO-L** exhibits a higher reactivity at higher concentrations in the initial first seconds but a concentration decrease obviously results in a faster drop of reactivity during the crosslinking process. Here, **CD-PI** exhibits more tolerance upon concentration changes.

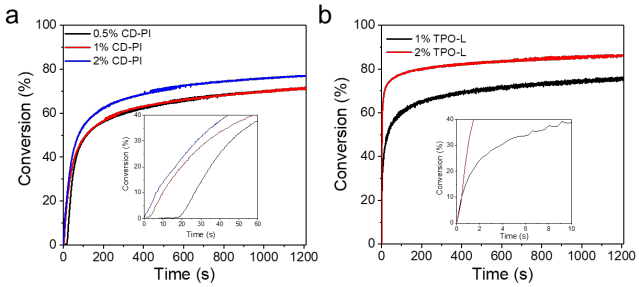

Figure 3. Polymerization kinetics represented by conversion-time profiles collected by real-time FTIR in the matrix of the monomer mixture (**UDMA** and **TPGDA** (60:40, wt%)) using a) **CD-PI** and b) **TPO-L** in different concentrations, respectively. The exposure was carried out using UV-LED emitting at 365 nm with an intensity of 200 mW/cm^2. The inset shows a cut of the respective kinetic traces in a shorter time frame.

This must impact material properties studied by dynamical analysis shown for the tan δ (Figure 4a) and the loss modulus (Figure 4b). Data obtained for tan δ indicate a lower glass transition temperature for **CD-PI**-based processed material than those with **TPO-L**. Nevertheless, a shoulder appears to indicate a second glass transition temperature, which indicates a phase-separated network in the latter case. Surprisingly, this does not clearly appear in the case of **CD-PI**. Both tan δ and loss modulus data show an almost homogeneous network as indicated by one glass transition temperature. This can be seen as an interesting feature for future developments. Homogeneous networks should also exhibit less brittleness, which can be seen as a big feature for future developments.

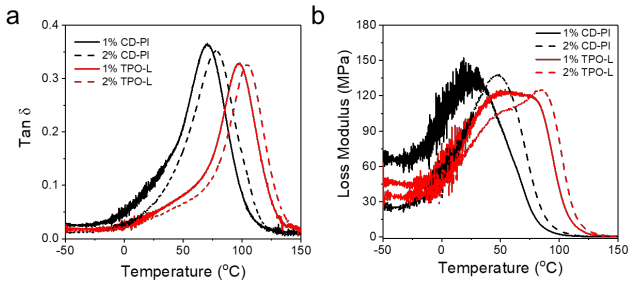

Figure 4. DMA profiles of a) tan δ and b) Loss Modulus of the polymer films obtained by exposure with UV-LED emitting at 365 nm for 15 mins using the monomer mixture (**UDMA** and **TPGDA** (60:40, wt)).

Table 1 summarizes data obtained for DMA analysis regarding T_g evaluated from storage modulus (Figure S13-S16), loss modulus, and tan δ. A comparison between network densities available from the storage modulus of materials processed by either **CD-PI** or **TPO-L** cannot be made due to the heterogeneous appearance of the networks obtained by **TPO-L** as **PI**. The multi-functional structural pattern of the **CD-PI** causes a different network structure compared to a traditional **PI**; that is **TPO-L**. In the case of **CD-PI**, bond cleavage results in the formation

of a low molecular weight radical (Ar·) and the carbon dot comprising many iminyl radicals at the surface (see the pattern of **CD-PI** in Figure 1). The latter exhibits significantly higher molecular weight and, therefore, less mobility. Thus, monomers adding to the iminyl radical decorated at the surface of the **CD** shall possess lower mobility resulting in a decrease in the polymer radical mobility compared to radicals generated by **TPO-L**. Consequently, the efficiency of termination should decrease. Such radical structures should possess less mobility, explaining their possibly lower reaction rate in the termination process. Thus, such networks formed by multi-functional **CD-PI** obviously possess larger M_c between two network junctions and consequently lower network density. As a result, the growing polymer radical chains, which propagate from the star-shaped initiator, terminate later because of the lower probability of finding a terminating radical, resulting in a larger M_c as explained by the lower glass transition temperature. In other words, the star-shaped structure of initiating moieties causes a later termination resulting in larger M_c. The remaining low molecular aryl radical may contribute to primary radical termination, explaining the large tolerance of initiator variation shown in Figure 3.

PI	Conc. (wt%)	Tg (E') (°C)	Tg (E'') (°C)	Tg (tan δ) (°C)	E'(Tg) (MPa)
CD-PI	1	-25	26	70	2206
CD-PI	2	-15	47	78	1267
TPO-L	1	-12	50, 75	97	1754
TPO-L	2	-2	48, 83	104	a)

Table 1. Summary of material data obtained by photoinduced polymerization of a mixture of **UDMA**:**TPGDA**=60:40 using different **PI** concentrations with an LED emitting at 365 nm.
[a)]: not possible to determine due to the overlap of two transitions.

An additional advantage of **CD-PI** as Type I **PI** can be seen in good biocompatibility (Figure S17). Nearly negligible cellular death occurred by an increase up to 400 □g/mL, indicating a better performance compared to **TPO-L**. This interesting feature gives some hope for future uses in biomedical applications where the achievement of large curing thickness represents one big challenge such as in dental restauration[26]. The curing depth with samples comprising **CD-PI** was checked without deoxygenated treatment. A linear dependence existed between exposure time up to 30 min resulting in curing depth of ~25 mm. An increase of exposure to 60 min increased the curing depth again, resulting in ~30 mm depth of curing (Figure **S18**).
Performance in photopolymerization can be additionally increased by selection of an alternative carbon precursor; that is 5-Hydroxymethylfurfural (**HMF**) to prepare the carbon dot resulting finally in **HMF**-based **CD-PI** (**CD-PI-HMF**). They obviously showed enhanced absorbance between 300-400 nm enabling **CD-PI-HMF** to improve photoinitiating performance compared to **CD-PI** (Figure S19). Further investigations will be pursued to find out which specific structural feature formed in the hydrothermal treatment contributes to the improvement of photoinitiating efficiency. The result obtained demonstrates that CH_2OH groups obviously appear more effective as CHO groups bound on the furane moiety to make the **CD** in a hydrothermal procedure (Figure 1).
These interesting features address to check the migration behavior of non-reacted photoinitiators. Quantification of migrated **CD-PI** or **TPO-L** was determined by UV-Vis. spectra using cured samples, which were immersed in ethanol, as target material (Figure S20). Compared to the sample processed by **TPO-L**, films prepared by **CD-PI** exhibited a lower migration rate in ethanol (**Figure 5**). Interestingly, there was no **CD-PI** measurable at the beginning while samples prepared by **TPO-L** exhibited remarkable amount of **PI** that already migrated. In addition, longer storage in ethanol indicated a much stronger increase in migration ratio in the case of **TPO-L**. These interesting results will give some new impetus to develop

PI with lower migration ratio for the future. Particularly applications requesting low emissions will benefit from the features of these new materials introduced here.

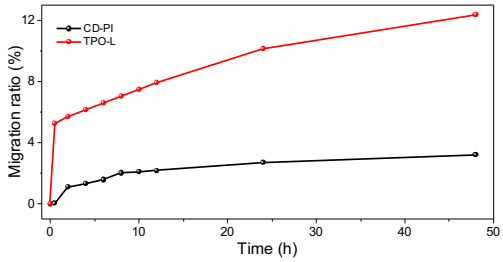

Figure 5. Migration ratio of the film (**UDMA** and **TPGDA** (60:40, wt)) cured by **CD-PI** and TPO-L in ethanol for different times. **SI** compiles details about experimental conditions.

More information is also available at: 10.1002/anie.202404454.

Conclusion

These results enable to conclude that type I radical photoinitiators based on sustainable carbon dots originating from furfural exhibit interesting features regarding the formation of polymer networks. The use of such **PI** to crosslink multi-functional monomers results in polymer networks showing more homogeneity compared to traditional **PI**s. The star-shaped structural pattern of photocleavable oxime ester groups on the surface of the sustainable carbon dot responsibly initiates radical polymerization in several directions if the absorption of more than one photon proceeds in separate events. This leads to more tolerance against changes in **PI** concentration, less chain termination, and, therefore, less inhomogeneity, as confirmed by the DMA. Such features will definitively impact further developments considering practical uses in different fields of light-mediated crosslinking based on radical polymerization.

The use of the oxime ester structures also addresses continuing research in this field. Here, further structural elements that may affect the bond stability of the oxime ester might be of interest. Thus, the replacement of aryl moieties by heterocyclic moieties will bring additional impetus in this field to improve photolytic cleavage efficiency and absorption in the UV-A. Desirable would be a more bathochromic shifted absorption to enable alternative LED wavelengths at 385/395 nm, and 405/410 nm LEDs, or even higher wavelength in the blue part at 470 nm to bring them as alternatives to dental applications. The fact that migration issues decreased brings interesting features to the many applications mentioned in the introduction wherever humans would be in contact with the material. Finally, photophysical measurements such as flash spectroscopy definitively will bring more knowledge into the field to study the reactivity of the radicals formed at the **CD**.

References

[1] a)S. Dadashi-Silab, S. Doran, Y. Yagci, *Chem. Rev.* **2016**, *116*, 10212-10275. b)X. He, L. Zang, Y. Xin, Y. Zou, *Applied Research* **2023**, *2*, e202300030. c)X. Luo, Y. Zhai, P. Wang, B. Tian, S. Liu, J. Li, C. Yang, V. Strehmel, S. Li, K. Matyjaszewski, G. Yilmaz, B. Strehmel, Z. Chen, *Angew. Chem, Int. Ed.* **2023**, e202316431. d)K. Sun, Y. Zhang, D. Zhu, X. Peng, J. Zhang, T. Gong, M. Ma, P. Xiao, *J. Photochem. Photobiol. C* **2023**, *57*, 100637. e)N. Corrigan, J. Yeow, P. Judzewitsch, J. Xu, C. Boyer, *Angew. Chem., Int. Ed.* **2019**, *58*, 5170-5189. f)U. Kolczak, G. Rist, K. Dietliker, J. Wirz, *J. Am. Chem. Soc.* **1996**, *118*, 6477-6489. 10.1021/ja9534213. g)W. Rutsch, K. Dietliker, d. Leppard, M. Koehler, L. Misev, U. Kolczak, G. Rist, *Prog. Org. Coat.* **1996**, *27*, 227-239. 10.1016/0300-9440(95)00539-0. h)K. Dietliker, T. Jung, J. Benkhoff, H. Kura, A. Matsumoto, H. Oka, D. Hristova, G. Gescheidt, G. Rist, *Macromol. Symp.* **2004**, *217*, 77-98. i) Z. Li, X. Zou,

F. Shi, R. Liu, Y. Yagci, *Nat. Comm.* **2019**, *10*, 3560. j)B. Strehmel, C. Schmitz, C. Kütahya, Y. Pang, A. Drewitz, H. Mustroph, *Beilstein Journ.Org. Chem.* **2020**, *16*, 415-444.

[2] a)H. Baumann, T. Hoffmann-Walbeck, W. Wenning, H.-J. Lehmann, C. D. Simpson, H. Mustroph, U. Stebani, T. Telser, A. Weichmann, R. Studenroth, "Imaging Technology, 3. Imaging in Graphic Arts", in ″Imaging Technology, 3. Imaging in Graphic Arts″, Wiley-VCH Verlag GmbH & Co. KGaA, **2015**, pp. 1-51. b)H. Baumann, "Lithographische Druckplatten für Laserbelichtung", *Chemie in unserer Zeit* **2015**, *48*, 14-29. 10.1002/ciuz.201400642. c)B. Strehmel, S. Ernst, K. Reiner, D. Keil, H. Lindauer, H. Baumann, *Z. Phys. Chem.* **2014**, *228*, 129-153.

[3] a)X. Allonas, B. Hammouda, B. Métral, E. Goldbach, A.-S. Schuller, C. Ley, C. C. Croutxé-Barghorn, *Applied Research* **2024**, e202400004. b)S. C. Gauci, A. Vranic, E. Blasco, S. Bräse, M. Wegener, C. Barner-Kowollik, *Adv. Mater.* **2023**, 2306468. c)Z. Zhang, N. Corrigan, C. Boyer, *Angew. Chem., Int. Ed.* **2022**, *61*, e202114111. d)C. Vazquez-Martel, P. Mainik, E. Blasco, *Organic Materials* **2022**, *4*, 281-291. e)S. C. Ligon, R. Liska, J. Stampfl, M. Gurr, R. Mülhaupt, *Chem. Rev.* **2017**, *117*, 10212-10290. f)J. Zhang, P. Xiao, "3D printing of photopolymers", *Polym. Chem.* **2018**, *9*, 1530-1540.

[4] a)F.-K. Bruder, R. Hagen, T. Rölle, M.-S. Weiser, T. Fäcke, *Angew. Chem., Int. Ed.* **2011**, *50*, 4552-4573. b)A. Ibrahim, X. Allonas, C. Ley, K. Kawamura, H. Berneth, F.-K. Bruder, T. Fäcke, R. Hagen, D. Hoenel, T. Rölle, G. Walze, M. S. Weiser, *Chem. - Eur. J.* **2014**, *20*, 15102-15107. c)F.-K. Bruder, T. Fäcke, T. Rölle, *Polymers* **2017**, *9*, 472/471-472/435.

[5] I. Lamparth, P. Fassler, T. Schnur, E. Thetiot, J. Lalevee, Y. Catel, *Dent. Mater.* **2022**, *38*, 1108-1116.

[6] a)P. Mischke, B. Strehmel, "Filmbildung″, Vincentz Network, Hannover, **2018**. b)L. Appelhoff, Q. Wang, B. Strehmel, "Colorless surface coatings″, WO2022200192, (Hochschule Niederrhein), **2022**. c)B. Stremel, L. Appelhoff, T. Brömme, E. Oks, "Near-infrared light curable aqueous coating composition″, WO2023241904, (Altana AG), **2023**.

[7] a)Q. Wang, S. Popov, V. Strehmel, J. S. Gutmann, B. Strehmel, *Polym. Chem.* **2023**, *14*, 116-125. b)Y. Pang, A. Shiraishi, D. Keil, S. Popov, V. Strehmel, H. Jiao, J. S. Gutmann, Y. Zou, B. Strehmel, *Angew. Chem., Int. Ed.* **2021**, *60*, 1465-1473. c)Y. Xin, S. Xiao, Y. Pang, Y. Zou, *Prog. Org. Coat.* **2021**, *153*, 106149.

[8] H. Lai, X. Peng, L. Li, D. Zhu, P. Xiao, *Prog. Polym. Sci.* **2022**, *128*, 101529.

[9] L. Hongbo, "Current Situation and Development Trend of Radiation Curing in China", in *The 30th Anniversary Commemorative Conference on Radiation Curing*, Radtech China, Yixing, **2023**.

[10] a)A. Lago, A. Rodríguez-Bernaldo de Quirós, R. Sendón, J. Bustos, M. T. Nieto, P. Paseiro, *Food Additives & Contaminants: Part A* **2015**, 1-20. b)B. Zeng, Z. Cai, J. Lalevée, Q. Yang, H. Lai, P. Xiao, J. Liu, F. Xing, *Toxicology in Vitro* **2021**, *72*, 105103.

[11] Y. Wu, R. Li, J. Wang, Y. Situ, H. Huang, *J. Polym. Sci.* **2022**, *60*, 52-61.

[12] Y. Wu, C. Dai, J. Ke, R. Tang, C. Huang, J. Wang, Y. Situ, H. Huang, *Progr. Org. Coat.* **2023**, *176*, 107396.

[13] a)Y. Zhu, L. Li, Y. Zhang, Y. Ou, J. Zhang, Y. Yagci, R. Liu, *Prog. Org. Coat.* **2023**, *174*, 107272. b)Z. Liu, F. Dumur, *Eur. Polym. J.* **2022**, *177*, 111449. c)S. Fan, X. Sun, X. He, Y. Pang, Y. Xin, Y. Ding, Y. Zou, *Polymers* **2022**, *14*, 4588. d)F. Dumur, *Eur. Polym. J.* **2022**, *163*, 110962. e)R. Zhou, X. Sun, R. Mhanna, J.-P. Malval, M. Jin, H. Pan, D. Wan, F. Morlet-Savary, H. Chaumeil, C. Joyeux, *ACS Appl. Polym. Mater.* **2020**, *2*, 2077-2085. f)D. E. Fast, A. Lauer, J. P. Menzel, A.-M. Kelterer, G. Gescheidt, C. Barner-Kowollik, *Macromolecules* **2017**, *50*, 1815-1823.

[14] a)Y. Zhang, Z. Liu, T. Borjigin, B. Graff, F. Morlet-Savary, M. Schmitt, D. Gigmes, F. Dumur, J. Lalevee, *Green Chem.* **2023**, *25*, 6881-6891. 10.1039/d3gc02004e.b)H. Chen,

D. Zhu, T. Kavalli, P. Xiao, M. Schmitt, J. Lalevee, *Polym. Chem.* **2023**, *14*, 3543-3568. d)G. Noirbent, F. Dumur, *Eur. Polym. J.* **2021**, *142*, 110109.

[15] a)H. Guo, M. Cao, R. Liu, B. Tian, S. Liu, J. Li, S. Li, B. Strehmel, T. D. James, Z. Chen, *Nat. Comm.* **2024**, *15*, 1590. b)X. Luo, Y. Zhai, P. Wang, B. Tian, S. Liu, J. Li, C. Yang, V. Strehmel, S. Li, K. Matyjaszewski, G. Yilmaz, B. Strehmel, Z. Chen, *Angew. Chem. Int. Ed.* **2023**, e202316431. c)X. Guo, X. Zhao, X. Luo, Y. Pang, B. Tian, S. Liu, S. Li, J. Li, B. Strehmel, Z. Chen, *Angew .Chem. Int. Ed.* **2023**, *62*, e202301242. d)C. Kütahya, Y. Zhai, S. Li, S. Liu, J. Li, V. Strehmel, Z. Chen, B. Strehmel, *Angew. Chem. Int. Ed.* **2021**, *60*, 10996. e)C. Kütahya, P. Wang, S. Li, S. Liu, J. Li, Z. Chen, B. Strehmel, *Angew. Chem., Int. Ed.* **2020**, *59*, 3166-3171. 10.1002/anie.201912343.

[16] a)C. Wu, N. Corrigan, C. H. Lim, W. Liu, G. Miyake, C. Boyer, *Chem. Rev.* **2022**, *122*, 5476-5518. b)N. Corrigan, K. Jung, G. Moad, C. J. Hawker, K. Matyjaszewski, C. Boyer, *Prog. Polym. Sci.* **2020**, *111*, 101311.

[17] C. Schmitz, T. Poplata, A. Feilen, B. Strehmel, *Progr. Org. Coat.* **2020**, *144*, 105663.

[18] a)W. Meng, X. Bai, B. Wang, Z. Liu, S. Lu, B. Yang, *Energy Environ. Mater.***2019**, *2*, 172-192. b)X. Zhang, M. Jiang, N. Niu, Z. Chen, S. Li, S. Liu, J. Li, *ChemSusChem* **2018**, *11*, 11-24.

[19] L. Đorđević, F. Arcudi, M. Cacioppo, M. Prato, *Nat. Nanotechnol.* **2022**, *17*, 112-130.

[20] C. R. J. Stephenson, T. P. Yoon, D. W. C. MacMillan, "Visible Light-Active Photocatalysis″, Wiley-VCH, **2018**.

[21] a)B. Wang, H. Song, X. Qu, J. Chang, B. Yang, S. Lu*, Coord. Chem. Rev.* **2021**, *442*, 214010. b)Z. Wang, W. Tu, Y. Zhao, H. Wang, H. Huang, Y. Liu, M. Shao, B. Yao, Z. Kang, J Mater Chem A. **2020**, *8*, 14566-14573. c)X. Bao, Y. Yuan, J. Chen, B. Zhang, D. Li, D. Zhou, P. Jing, G. Xu, Y. Wang, K. Holá, D. Shen, C. Wu, L. Song, C. Liu, R. Zbořil, S. Qu, *Light sci. appl.* **2018**, *7*, 91.

[22] S. Gayathri, P. Viswanathamurthi, R. Bertani, P. Sgarbossa, *ACS Omega* **2022**, *7*, 33107-33122.

[23] a)E. G. Janzen, C. A. Evans, *J. Amer. Chem. Soc.* **1975**, *97*, 205-206. b)G. R. Buettner, *Free Radical Biology and Medicine* **1987**, *3*, 259-303.

[24] J. Yue, L. Li, C. Jiang, Q. Mei, W.-F. Dong, R. Yan, *J. Mat. Chem. B* **2021**, *9*, 7972-7978.

[25] a)L. Zhang, C. Wu, K. Jung, Y. H. Ng, C. Boyer, *Angew. Chem. Int. Ed.* **2019**, *58*, 16811-16814. b)Z. Wu, T. Zhang, X. Shi, N. Corrigan, G. Ng, C. Boyer, *Angew. Chem., Int. Ed.* **2023**, *62*, e202302451.

[26] a)S. Keck, O. Liske, K. Seidler, B. Steyrer, C. Gorsche, S. Knaus, S. Baudis, *Biomacromolecules* **2023**, *24*, 1751-1762. b)S. M. Müller, S. Schlögl, T. Wiesner, M. Haas, T. Griesser, *ChemPhotoChem* **2022**, *6*, e202200091. c)Y. Zhang, L. Josien, J.-P. Salomon, A. Simon-Masseron, J. Lalevee, *ACS Appl. Polym. Mater.* **2021**, *3*, 400-409. d)R. Liu, X. Zou, Y. Xu, X. Liu, Z. Li, *Chem. Lett.* **2016**, *45*, 1054-1056. 10.1246/cl.160534.